Journal of Power Sources 196 (2011) 5386–5393

Contents lists available at ScienceDirect

Journal of Power Sources

journal homepage: www.elsevier.com/locate/jpowsour

Pulsed plasma-polymerized alkaline anion-exchange membranes for potential application in direct alcohol fuel cells

Chengxu Zhang[a,d], Jue Hu[a,*], Jie Cong[a], Yanping Zhao[a], Wei Shen[a], Hirotaka Toyoda[b], Masaaki Nagatsu[c], Yuedong Meng[a]

[a] Institute of Plasma Physics, Chinese Academy of Sciences, P.O. Box 1126, Hefei, PR China
[b] Department of Electrical Engineering and Computer Science, Nagoya University, Chikusa, Nagoya, Japan
[c] Nanovision Science Section, Graduate School of Science and Technology, Shizuoka University, Naka-ku, Hamamatsu, Japan
[d] Department of Modern Physics, University of Science and Technology of China, Hefei, PR China

ARTICLE INFO

Article history:
Received 21 January 2011
Received in revised form 20 February 2011
Accepted 21 February 2011
Available online 26 February 2011

Keywords:
Pulsed plasma polymerization
Alkaline anion-exchange membrane
Direct alcohol fuel cells
Quaternized poly(vinylbenzyl chloride)
Ultra-thin films

ABSTRACT

Pulsed plasma polymerization is adopted to synthesize alkaline anion-exchange membranes (AAEMs) with high contents of functional groups. The attenuated total reflection Fourier transform infrared spectroscopy, X-ray photoelectron spectroscopy and thermo gravimetric analysis demonstrate that the benzyltrimethylammonium cationic groups can be successfully introduced into the polymer matrix. The content of the quaternary nitrogen in pulsed plasma-polymerized membrane is up to 1.93 atom%. The ultra-flat and undamaged morphology structure of the AAEMs indicates a low plasma ablation effect in the pulsed plasma polymerization. The excellent properties of the pulsed plasma-polymerized AAEMs, including good adhesion to the substrate, acceptable chemical stability and thermal stability, high ion-exchange capacity (1.42 mmol g^{-1}) and water uptake (59.73 wt%), interesting ionic conductivity (0.0205 S cm^{-1} in deionized water at 20 °C) and ethanol permeability (3.37×10^{-11} m^2 s^{-1}), suggest a great potential for application in direct alcohol fuel cells.

1. Introduction

In recent years, interest has grown in the development of alkaline direct alcohol fuel cells (ADAFCs) for stationary and mobile applications due to the highly efficient electric power generation, the low overpotentials and the potential to forego noble metal catalysts [1–5]. Alkaline anion-exchange membranes (AAEMs), which serve dual functions of hydroxide ion conducting and fuels separating, can seriously affect the performance of ADAFCs. The need for AAEMs with the necessary conductivity, alcohol permeability, thermal stability and chemical stability is a key challenge in the development of ADAFCs. Although, previous studies have successfully fabricated AAEMs with high conductivity and excellent stability, it is difficult to synthesize AAEMs with several micrometers thickness due to the restriction of the traditional film-casting method [6–10]. Considering the mobility of hydroxide ions is inherently slower than that of proton in dilute solution, the property of AAEMs with ultra-thin structure is also promising [11]. Herein, plasma polymerization was adopted to prepare AAEMs. The scheme of fabricating AAEM and novel membrane electrode assembly (MEA) for application in the ADAFC using plasma polymerization technique is shown in Fig. 1. Plasma polymerization technique is promising to prepare ion-exchange membranes with a few microns thickness, highly cross-linked backbone structure, and good adhesion to the substrate. The highly cross-linked structure can improve the membrane chemical and mechanical properties. The strong adhesion to the electrode by directly depositing membrane onto catalyst layer will decrease the interfacial resistance between membrane and electrode, further improving the performance of ADAFCs.

Vinylbenzyl chloride (VBC) is an excellent monomer for synthesis of AAEMs for having two functional groups: vinyl group for polymerization reaction and benzyl chloride group for quaternization. There are mainly two steps in fabrication of plasma polymerized alkaline anion-exchange membrane using VBC as monomer: (1) plasma polymerization of VBC monomer into poly(vinylbenzyl chloride); (2) quaternization of benzyl chloride groups into $-N^+(CH_3)_3OH^-$ groups. Because of the low bond dissociation energy of the C–Cl bond in benzyl chloride groups, it is very hard to synthesize plasma-polymerized membrane with high contents of benzyl chloride groups. The after-glow discharge plasma polymerization (AGD-PP) system allows lower destruction of membranes by plasma ablation effect, and higher preservation of the membranes structure. However, in our previous studies, the plasma ablation is obvious even in AGD-PP system [12]. It is believed that a variety of reactive species (e.g. ion and neutral radicals, etc.)

* Corresponding author. Tel.: +86 551 5591378; fax: +86 551 5591310.
E-mail address: hujue@ipp.ac.cn (J. Hu).

0378-7753/$ – see front matter © 2011 Elsevier B.V. All rights reserved.
doi:10.1016/j.jpowsour.2011.02.073

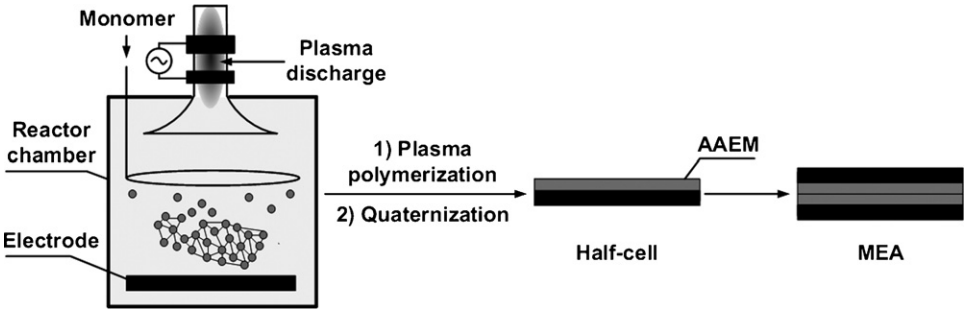

Fig. 1. Schematic diagram for synthesis of alkaline anion-exchange membrane and membrane electrode assembly by plasma polymerization.

are produced during the plasma on periods and consumed during plasma off periods. To decrease the plasma ablation effect, pulsed plasma-polymerization was firstly employed to prepare AAEMs.

The object of the present study is to prepare and characterize the novel pulsed plasma-polymerized AAEMs for potential application in ADAFCs.

2. Experimental

2.1. Materials

Potassium hydroxide (KOH, AR grade), sodium hydroxide (NaOH, AR grade), trimethylamine (NMe_3, 33 wt%), hydrochloric acid (HCl, 37 wt%) and ethanol (EtOH, 99.7 wt%) were obtained from Shanghai Chemical Reagent Store (China). Vinylbenzyl chloride (VBC, 95 wt%) was purcharsed from Alfa Aesar®, and used without further purification. AHA membrane (Cl^- form) received from NEOSEPTA was treated with 2 M KOH solution to convert the Cl^- form into OH^- form, and then stored in deionized water. Deionized water was used in all experiments.

2.2. Synthesis of plasma polymerized alkaline anion-exchange membrane

The plasma-polymerized membranes were synthesized in a pulsed after-glow discharge system, depicted in Fig. 2, consisting of a stainless steel reactor, a radio frequency (RF) power supply with corresponding power coupling system, a pulse modulation, a substrate bias voltage supply, a monomer heater with a temperature control system, gas mass flow controllers with flow indicators, vacuum system (a mechanical booster pump, a rotary pump and liquid nitrogen trap) with vacuum gauge. The reactor was in a after-glow discharge configuration, meaning that the glow discharge was produced in the upper part of the reactor (in a Pyrex glass tube) and the plasma polymerization was performed in the lower part of it (stainless steel chamber). The plasma discharge was sustained by a pulsed mode RF power supply between two external electrodes (5 cm gap) in the Pyrex glass tube using Ar (supplied by air liquid) as working gas. 4-Vinylbenzyl chloride monomer carried by H_2 (supplied by air liquid), was introduced into the polymerization region through an air distribution ring. The flow rates of Ar, VBC monomer and H_2 were controlled by gas mass flow controllers. In order to avoid the condensation and polymerization of monomer on the inner walls of the gas lines, heating wires were wrapped around them, as shown in Fig. 2. The liquid nitrogen trap was placed in front of the pumps to avoid erosion of the vacuum pumps by untreated monomer and byproducts of the plasma polymerization. The constant parameters in this experiment were 10% for the plasma duty cycle, 30 W for the discharge power, 60 Pa for the reactor total pressure (10 Pa for partial pressure of argon) and −10 V for the bias voltage to the substrate. There are different substrates used to support plasma-polymerized membrane: silicon wafers [p-doped Si(1 0 0)] for SEM observations and thermogravimetric analyses, stainless steel plates for chemical structural characterizations and polytetrafluoroethylene (PTFE) porous substrates for ionic conductivity and ethanol permeability measurements.

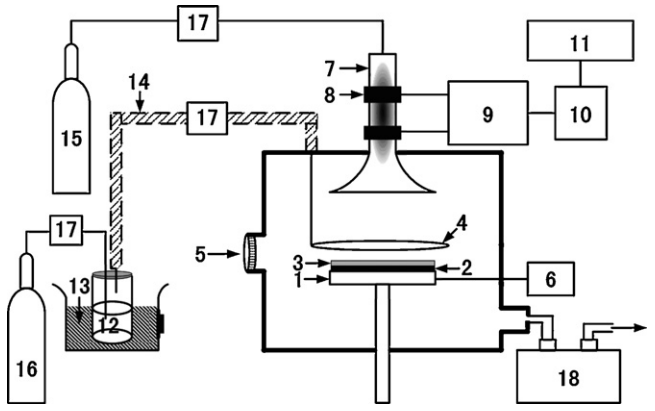

Fig. 2. Schematic diagram of the apparatus used for plasma polymerization. (1) Substrate holder, (2) substrate, (3) plasma polymerized membrane, (4) air distribution ring, (5) watch window, (6) bias voltage power source, (7) Pyrex glass tube, (8) electrode, (9) mathching network, (10) RF power supply, (11) pulse modulation, (12) liquid monomer in glass test tube, (13) water bath, (14) heating wires, (15) argon liquid gas to pump, (16) hydrogen liquid gas, (17) gas mass flowmeter and (18) rotary pump.

To quaternize of benzyl chloride groups into $-N^+(CH_3)_3OH^-$ groups, the plasma-polymerized vinylbenzyl chloride (PVBC) membranes were submerged in 33 wt % trimethylamine (TMA) aqueous solution for at least 48 h at room temperature. After soaking, the membranes (Cl^- form) were washed with deionized water to remove excess TMA solution. The treated membranes were immersed in 2 mol L^{-1} potassium hydroxide aqueous solution at room temperature for 48 h to convert the $-N^+(CH_3)_3Cl^-$ groups into $-N^+(CH_3)_3OH^-$ groups. Then, the quaternized poly(vinylbenzyl chloride) membranes (QPVBC) were washed by deionized water to remove any trapped potassium hydroxide and finally immersed in deionized water >48 h with frequent water changes.

2.3. Characterization of membranes

The morphology and microstructure of the plasma polymerized AAEM were observed by scanning electron microscope (SEM) (Sirion 200, FEI, USA) at operation voltage of 5.0 kV. In order to expose the cross-section, the QPVBC membrane with silicon substrate was frozen in liquid nitrogen and broken. Before observation, the membrane samples were sputtered with gold for several seconds since the plasma-polymerized membranes were nonconductive.

The chemical structure and composition of the PVBC and QPVBC membranes were analyzed by attenuated total reflection Fourier transform infrared spectroscopy (ATR-FTIR) and X-ray photoelectron spectroscopy (XPS). All the samples were dried in a vacuum oven at 60 °C for 12 h. The ATR-FTIR spectra of dried PVBC and QPVBC membranes were recorded using Nicolet NEXUS 870 spectrometer (Thermo Electron Corporation, USA) in the range of 4000–670 cm^{-1}. The spectra were obtained after 256 scans at 2 cm^{-1} resolution with subtracting the contributions from CO_2 and H_2O (gas). The XPS analysis was carried out using a Thermo ESCALAB 250 spectroscopy (Thermo Electron Corporation, USA) at a power of 150 W with a monochromatic Al Kα radiation at 1486.6 eV. The photoelectrons were detected with a hemispherical analyzer positioned at an angle of 90° with respect to the sample plane. XPS of PVBC and QPVBC membranes were recorded at pass energies of 70 eV for survey spectra and 20 eV for core level spectra. An additional electron gun was used to allow for surface neutralization during the measurements since the plasma polymerized membranes were nonconductive. The energy resolution was about 0.6 eV. The spectrometer energy scale calibration was checked by setting Ag $3d_{5/2}$ = 368.26 eV and the spectra were calibrated with respect to the C 1s peak at 284.6 eV. The curves were fitted with symmetrical Lorentz–Gauss functions.

Thermal degradation and stability of the membranes were investigated using a thermogravimetric analyzer (TGA) (DTG-60H, SHIMADZU, Japan). 12–16 mg dried membrane sample, placed in a Pt crucible, was heated from ambient temperature to 800 °C under flowing nitrogen at the scanning rate of 10 °C min^{-1}.

2.4. Ion-exchange capacity and water uptake measurements

In order to evaluate the capability of hydroxyl ion transport, the ion-exchange capacities (IECs) of PVBC and QPVBC membranes were measured by classical back titration method [13]. For IECs measurement, dry OH^- form samples were accurately weighed. Three pieces of dried membrane samples prepared in the same time were accurately weighed and then respectively equilibrated with 25 ml 0.005 mol L^{-1} HCl solution for 48 h and then back titrated by 0.005 mol L^{-1} NaOH solution. IEC values of the samples were calculated as the following relation

$$\text{IEC}\ \ (\text{mmol g}^{-1}) = \frac{n_{1,\text{HCl}} - n_{2,\text{HCl}}}{m_{dry}} \quad (1)$$

where m_{dry} is the mass (g) of the dried sample, $n_{1,HCl}$ and $n_{2,HCl}$ are the amount (mmol) of hydrochloric acid required before and after equilibrium, respectively. The average value of the three samples calculated from Eq. (1) is the IEC value of the measured membrane.

The water uptake of the PVBC and QPVBC membranes were carried out by measuring the change of weight between the membrane before and after immersion in deionized water. Firstly, the membrane was soaked in deionized water at room temperature and equilibrated for more than 48 h. The weight of the wet membrane was recorded as a benchmark by measuring after removing excess surface water. The wet membrane was then dried under vacuum at 60 °C until a constant weight was obtained. The water uptake could be calculated using Eq. (2)

$$\text{Water uptake}\,\% = \frac{m_{wet} - m_{dry}}{m_{dry}} \times 100\% \quad (2)$$

where m_{wet} is the mass (g) of a wet membrane and m_{dry} is the mass of a dry membrane.

2.5. Ionic conductivity measurements

The hydroxide ionic conductivity of the obtained membranes was measured by three-electrode AC impedance spectroscopy using an Autolab potentiostat/galvanostat (IM6e, Zahner, Germany) over a frequency ranging from 0.1 Hz to 1 MHz with oscillating voltage of 10 mV. Before conductivity measurements, the OH^- form of plasma polymerized membrane (QPVBC) samples (2.0 cm × 4.0 cm) and commercial AAEM (AHA, 2.0 cm × 4.0 cm) were fully hydrated in deionized water for at least 48 h until neutral pH was obtained. After removing the surface water, the hydrated membrane was then rapidly placed between two polytetrafluoroethylene (PTFE) plates, with the QPVBC membrane side contacted with three parallel platinum wires. The reference electrode (RE) was connected to the inner platinum wire, and the counter electrode (CE) and working electrode (WE) were connected to the outer two platinum wires, respectively. The testing cell was placed in a chamber with deionized water to keep the water content of the membrane constant during the measurements. The hydroxide ion conductivity σ_{OH^-} could be calculated by

$$\sigma_{OH^-}\ \ (\text{S cm}^{-1}) = \frac{l}{R_m A} \quad (3)$$

where A was the cross-sectional area (cm^2) of the membrane, l was the distance (cm) between the working electrode and reference electrode, R_m was the membrane resistance (Ω) obtained from the AC impedance data.

2.6. Ethanol permeability measurements

The ethanol permeability was measured by an open circuit potential method as reported in Refs. [14–17], using an Autolab potentiostat/galvanostat (IM6e, Zahner, Germany) at the temperature of 20 °C. Before testing, the OH^- form of plasma polymerized membrane QPVBC samples (3.0 cm × 3.0 cm) and AHA membrane (3.0 cm × 3.0 cm) were hydrated in deionized water for at least 48 h until neutral pH was obtained. The membrane sample was then clamped between two compartments of a diffusion cell by means of an O-ring seal with the membrane cross-sectional area of 2.0 cm^2 exposed to the solution. Teflon coated magnetic paddles were used in each compartment to ensure uniform mixing during the experiments. The compartment A as the donor compartment was loaded with 1 M KOH and 1 M EtOH solution. An equal volume of 1 M KOH solution was present in the compartment B (receptor compartment). In the compartment B, a Pt/C gas diffusion electrode (GDE) with flowing pure O_2, prepared by pasting Pt/C (40 wt%, Johnson Matthey) catalyst on carbon paper (Pt loading of 0.5 mg cm^{-2}), was used as WE [18]. A Pt foil was used as CE and a Hg/Hg_2Cl_2, KCl (saturated) electrode was used as RE. The ethanol permeability of the membrane can be estimated from the relationship between the concentration of ethanol in compartment B ($c_{EtOH,B}$ in mol L^{-1}) and the permeation time (t in s).

$$\frac{V_B L_m}{c_{\text{EtOH,A}} S} c_{\text{EtOH,B}}(t) = P\left(t + \frac{L_m^2}{6D}\right) \quad (4)$$

where P, D, L_m and S are the ethanol permeability (m^2 s^{-1}), diffusion coefficient (m^2 s^{-1}), membrane thickness (m) and membrane active area (m^2) of measured membrane, respectively. V_B and $c_{EtOH,A}$ are the volume of compartment B (m^3) and concentration of ethanol in compartment A (mol L^{-1}), respectively.

The ethanol concentration of compartment B can be estimated by the GDE potential drop from the calibration curve of potential shift against ethanol concentration. The method to establish the calibration curve of potential shift against ethanol concentration was described in our previous report, with substituting 1 M KOH solution for 0.5 M H_2SO_4 solution [14].

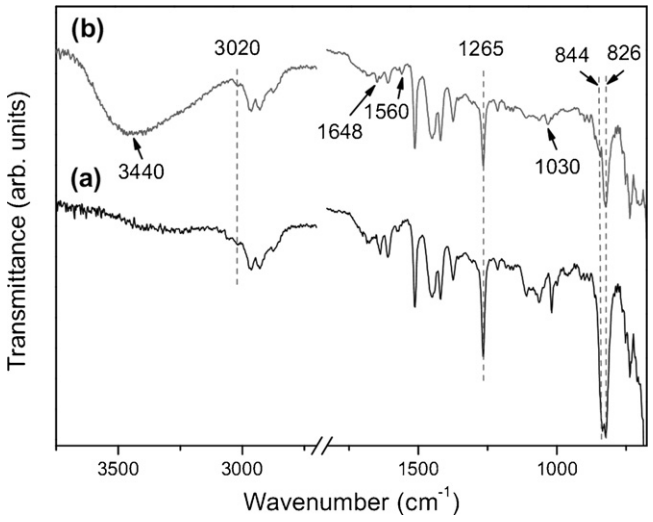

Fig. 3. ATR-FTIR spectra of (a) PVBC and (b) QPVBC membranes.

3. Results and discussion

3.1. Chemical structure characterization

The ATR-FTIR spectra of PVBC and QPVBC membranes deposited on stainless steel substrates at the duty cycle of 10%, discharge power of 30 W, total pressure of 60 Pa and bias voltage of −10 V were shown in Fig. 3. The ATR-FTIR spectra for both PVBC and QPVBC membrane were similar. The peaks appearing at 826 cm^{-1} and 3020 cm^{-1} are associated with the C–H deformation for para-substituted aromatics and aromatic C–H stretches, respectively, suggesting the existence of the benzene ring structure in PVBC and QPVBC membranes [19,20]. The absorption at 1265 cm^{-1} and 844 cm^{-1} attributed to CH_2–Cl wag of benzyl chloride groups and C–Cl stretching vibrations, respectively, indicate the preservation of the benzyl chloride groups in pulsed after-glow discharge system [21,22]. The bands at 1030 cm^{-1}, 1560 cm^{-1}, 1648 cm^{-1} and 3440 cm^{-1} of QPVBC membrane, not present in the spectra of the PVBC membrane, were assigned to hydroxyl group, C–N bonds, amide I band and OH stretching, respectively, indicating the successful quaternization of benzyl chloride groups into $-N^+(CH_3)_3OH^-$ groups [23–25].

XPS analysis was performed to determine the chemical structure of the obtained membrane. The XPS results of PVBC and QPVBC membranes with the contents of carbon, oxygen, chlorine and nitrogen expressed as atom %, were shown in Table 1. For PVBC membrane before quaternization, the nitrogen and oxygen atoms come from air contamination during and after plasma polymerization process. As shown in Table 1, the contents of oxygen and nitrogen increase after the quaternization processes, while the content of chlorine decreases, indicating the conversion of benzyl chloride groups into $-N^+(CH_3)_3OH^-$ groups. To acquire more information on the chemical structure characteristics of obtained membranes, XPS core level spectra of PVBC and QPVBC membranes were conducted. As regards the C 1s peak decomposition, shown in Fig. 4(a) and (b), four main components are detected in these spectra [26–29], which appear at 284.3 eV related to the sp^2 carbon atoms (C=C), 284.8 eV corresponded to the sp^3 carbon atoms (C–C and C–H), 286.1 eV attributed to sp^3 carbon bonded to one oxygen atom (C–O), chlorine atom (C–Cl) and nitrogen atom (C–N), and 287.2 eV assigned to the oxygenated groups (carbonyl). The increase in the C–N, C–O and C–Cl fraction in absorption at 286.1 eV and decrease in the content of chlorine of QPVBC membrane suggests the quaternization of PVBC membrane. In order to characterize the changes in the contents of benzyl chloride groups, the Cl 2p core-level spectra of the samples were curve-fitted with two spin–orbit–split doublets, shown in Fig. 4(c) and (d), with the binding energy for Cl $2p_{3/2}$ peak components located at 199.9 ± 0.2 eV attributable to the covalently bonded chlorine species in benzyl chloride groups, and 197.2 ± 0.2 eV related to the ionic chloride (Cl^-) [26,30,31]. The high content of covalently bonded chlorine species in PVBC membrane confirms that our choice of pulsed plasma polymerization can highly preserve the functional groups in polymerization progress. The decrease of the covalently bonded chlorine species contents verify the successful quaternization of benzyl chloride groups into $-N^+(CH_3)_3OH^-$ groups. However, the residual benzyl chloride groups and ionic chloride in QPVBC membrane, according to Fig. 4(d), indicates the incomplete quaternization. This difficulty for complete quaternization may be due to the high corss-linked C–C backbone and dense structure of the plasma-polymerized membrane. The existence of quaternary nitrogen groups can be further demonstrated by the decomposition of N 1s spectrum, shown in Fig. 4(f). The results of N 1s spectra analyses are in good agreement with what shown by Cl 2p spectra. The peaks of N 1s spectrum at 401.7 eV and 399.2 eV for QPVBC membrane were attributed to the quaternary or protonated nitrogen (N^+) and C–N bonds, respectively, confirming that plasma polymerization and quaternization could produce the expected anion-exchange groups in AAEM [32–35]. Quantitatively analysis of the N 1s spectrum of QPVBC membrane, shown in Table 1 and Fig. 4(f), reveals that the percentage of quaternary nitrogen with respect to the total atom quantity is 1.93% for plasma-polymerized alkaline anion-exchange membrane, which is higher than that of sulfonic acid groups for Nafion 117 membrane, shown as 1.23% in Ref. [14]. The high percentage of quaternary ammonium functional groups, attributed to the high preservation of benzyl chloride groups in plasma polymerization, indicates high ion conductivity of the pulsed plasma-polymerized AAEM and, as a result, a good performance in ADAFCs application. The high content of C–N bond in QPVBC membrane due to the trapped TMA indicates the high corss-linked C–C backbond and dense structure of the plasma-polymerized membrane.

Table 1
XPS elemental analysis of plasma-polymerized PVBC and QPVBC membranes deposited at plasma cycle duty of 10%, total pressure of 60 Pa, discharge power of 30 W, and bias voltage of −10 V.

Membrane	C (atom %)	O (atom %)	Cl (atom %)	N (atom %)	N^+ (atom %)
PVBC	84.98	10.18	3.89	0.96	0
QPVBC	76.30	17.72	0.74	4.79	1.93

3.2. Morphology of plasma polymerized AAEM

The surface and cross-section morphology of pulsed plasma polymerized QPVBC membrane deposited on silicon wafer can be recorded by SEM images, shown in Fig. 5. The QPVBC membrane is ultra-flat, ultra-thin, dense and free from defects with a uniform structure at the level of the SEM observation. The ultra-flat and undamaged morphology structure reflects the gentler deposition conditions involved and, in particular, absence of high-energy molecule–surface impact collisions thus suggesting a low plasma ablation effect in the pulsed plasma polymerization. This observation is crucial because the surface morphology structure of AAEM can directly influence the contact between two membranes, the interfacial resistance between two half-cells, and as a result, the performance of the fuel cell. The thickness of the QPVBC membrane is only 1.36 μm. From the cross-sectional view in Fig. 5, after immersion in 33 wt% TMA solution, 2 M KOH solution and deionized water for several days, plasma-polymerized AAEM did not peel off from the substrate, indicating a strong adhesion of mem-

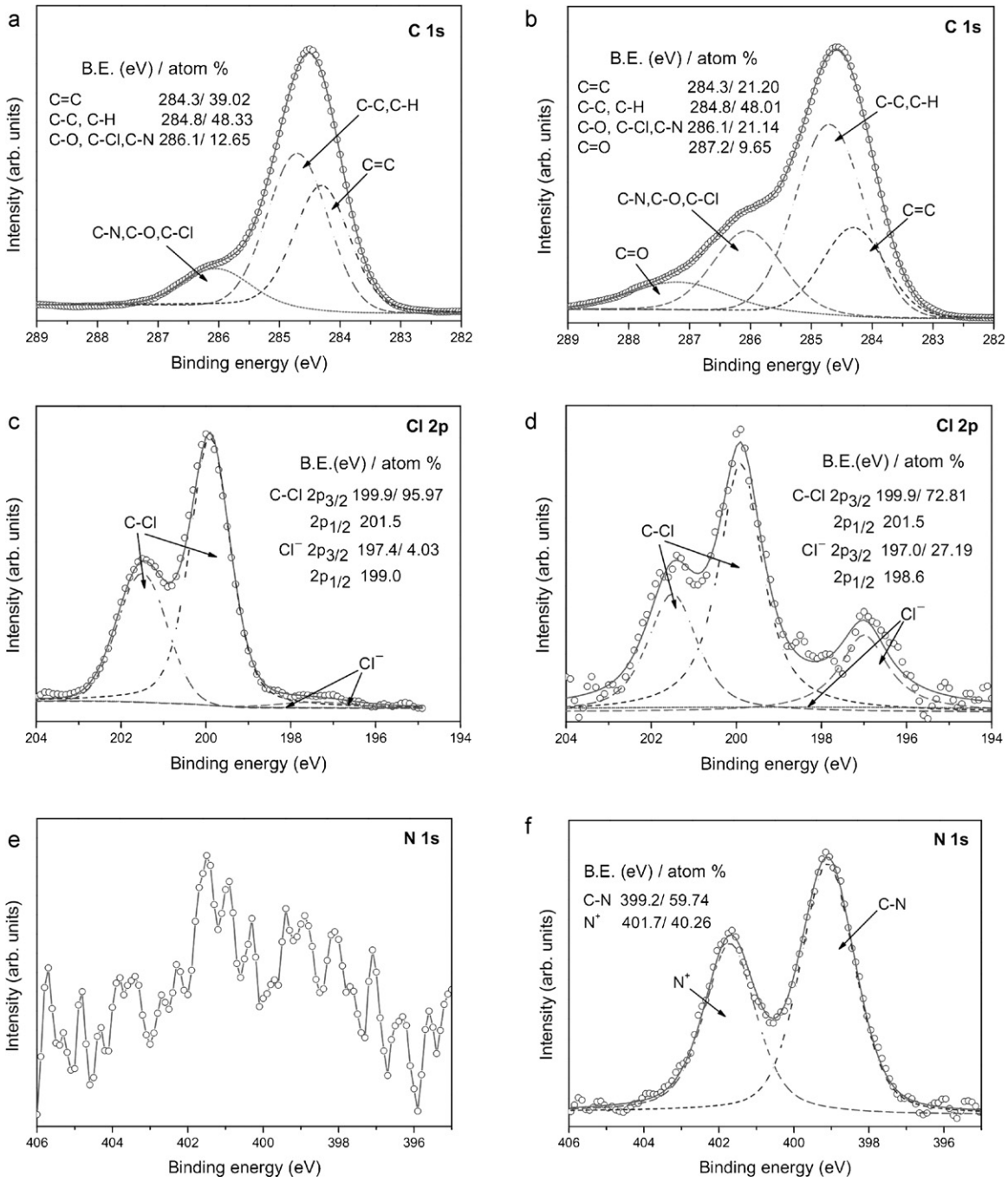

Fig. 4. XPS C 1s, Cl 2p and N 1s spectra for PVBC membrane (a, c and e) and QPVBC membrane (b, d and f).

brane to the substrate. This is significant for preparing membrane electrode assembly (MEA) with low interfacial resistance between membrane and electrodes. Good chemical stability of an AAEM based on quaternary ammonium groups is also desired. The SEM image displays the undamaged membrane structure in 2 M KOH solution for several days, indicating the high chemical stability of the obtained membrane [6].

3.3. Thermal stability

The thermal stability of PVBC and QPVBC membranes was investigated by TGA in flowing nitrogen from ambient temperature to 800 °C. In TGA trace, as shown in Fig. 6, the PVBC membrane is degraded mainly in the range of 270–500 °C, indicating the good thermal stability of PVBC membrane matrix due to the highly cross-linked structure [36]. The QPVBC membrane is stable below Exhibits 120 °C. The degradation in the range of 120–270 °C is corresponding to the loss of the benzyltrimethylammonium groups, suggesting a great stability of the resulting membrane below 120 °C. The second weight loss region of QPVBC membrane at temperature range of 270–460 °C ascribed to the degradation of the membrane main chain [37]. The thermal stability of the plasma polymerized AAEM was acceptable [6].

3.4. IEC and water uptake

IEC and water uptake are performed to determine the capability of hydroxide ion transport, and of course, to evaluate the

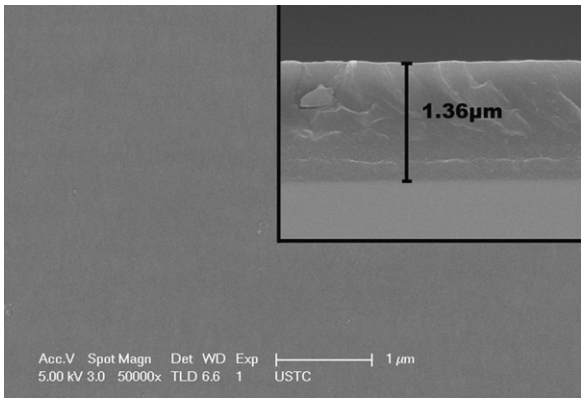

Fig. 5. SEM image of the QPVBC membranes on silica wafer [p-doped Si(1 0 0)]. The inset is a SEM image of the cross-section of it.

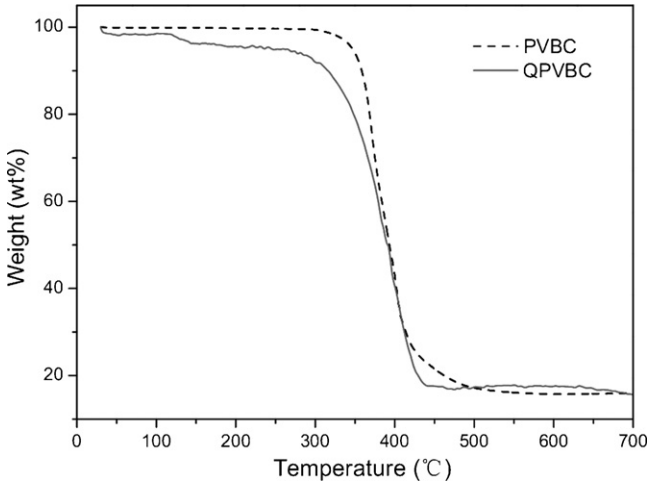

Fig. 6. Thermo gravimetric analyses of PVBC and QPVBC membranes.

applicability in ADAFCs of obtained membranes. IEC and water uptake values of the QPVBC membranes, included in Table 2, is found to be 1.42 mmol g^{-1} and 59.73 wt%, respectively, which is higher than that of PVBC membrane (0.27 mmol g^{-1} and 16.77 wt%, respectively), indicating the hydrophilic functional groups fixed in the polymer matrix. The high water uptake and IEC values of the alkalinized membrane could provide sufficient water molecules to transport OH^- ions through the membrane, indicating excellent ionic conductivity of the QPVBC membrane.

3.5. Ionic conductivity

Hydroxide ion conductivity of the AAEM is a crucial criterion for evaluating its performance in ADAFCs. Deionized water was used during ionic conductivity measurements in this work to evaluate the intrinsic nature of the polymer electrolyte. The ionic conductivity of the commercial AAEM (AHA OH^- form) was measured as the reference. Fig. 7(a) shows the Nyquist plot of ($-Z''$ vs. Z') for the QPVBC membrane, fitted by the equivalent circuit. The OH^- ion conductivity of QPVBC membrane (σ_{OH^-}), according to Eq. (3), is 0.0205 S cm^{-1} which is higher than that of the commercial AHA membrane (0.0035 S cm^{-1} close the value in Ref. [38]). The ionic conductivity of QPVBC membrane is in the order of 0.01 S cm^{-1}, indicating the satisfactory for application of the membrane in fuel cells [36]. This observation can be attributed to: (1) the high content of quaternary ammonium functional groups fixed in the QPVBC membrane matrix indicating the excellent hydrophilic property and the great potential for promoting conductivity; (2) the satisfactory IEC value (1.42 mmol g^{-1}) suggesting the high activity of the quaternary ammonium functional groups; (3) the high water uptake (59.73 wt%) leading to adequate water absorption in ion transport; and (4) the cross-linked structure resulting in the increase of ion incorporation [8,39].

Table 2
IEC and water uptake of the PVBC and QPVBC membranes.

Membrane	IEC (mmol g^{-1})	Water uptake (wt%)
PVBC	0.27	16.77
QPVBC	1.42	59.73

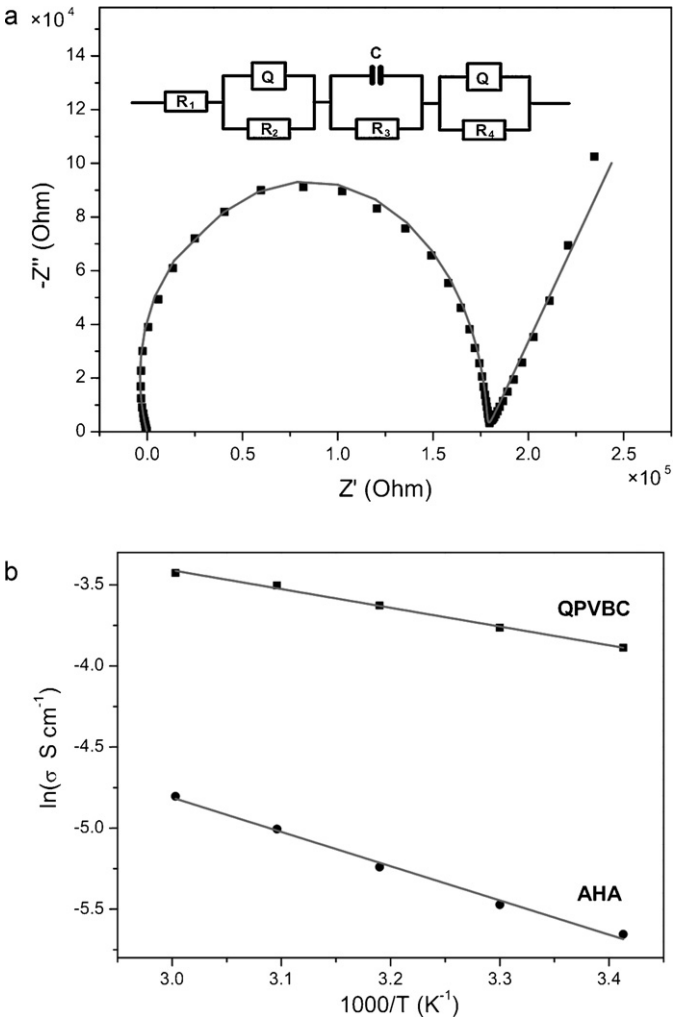

Fig. 7. (a) Nyquist plot for the QPVBC membrane and an equivalent circuit. The dots are the experimental results. The curves are the fitting of the experimental data using the equivalent circuit. (b) Arrhenius plot showing the temperature dependence of hydroxide conductivity for the QPVBC and AHA membranes.

Fig. 7(b) shows the correlation between conductivity and temperature for QPVBC and AHA membranes. The conductivity of the membranes increase with temperature and exhibit conductivities up to 60 °C when immersed in deionized water. Linear regression of $\ln \sigma_{OH^-}$ vs. $1000/T$ (T is the absolute temperature in Kelvins) was performed assuming an Arrhenius relationship. The anion transport activation energy (E_a), which corresponds to the energy barrier for carrier transfer from one free site to another, can be obtained according to the Arrhenius equation:.

$$E_a(\text{kJ mol}^{-1}) = RT^2 \frac{d \ln \sigma_{OH^-}}{dT} \quad (5)$$

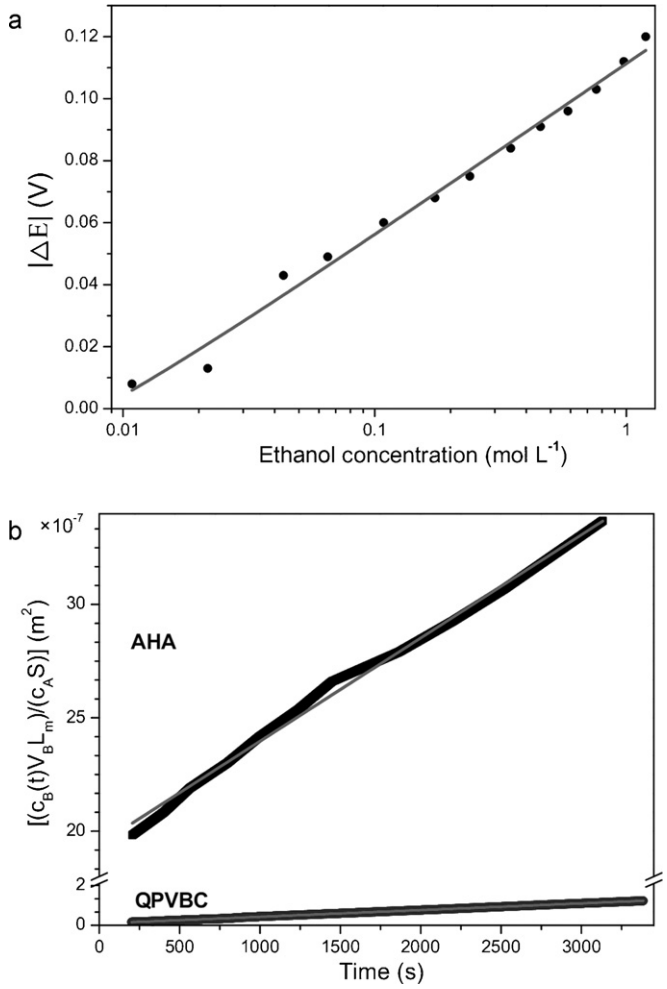

Fig. 8. (a) Potential shift against ethanol concentration. The dots are the experimental data and the line is the linear fitting of the experimental results using Eq. (6). (b) Permeability data for the QPVBC and AHA membranes in the ethanol concentration in compartment A of 1 mol L^{-1} at 20 °C.

where R is the pure gas constant (8.314 J K^{-1} mol^{-1}). The activation energy value for alkalinized QPVBC membrane is 9.61 kJ mol^{-1}, which is much lower than the value of AHA membrane (17.56 kJ mol^{-1}). The high conductivity and low ion transport activation energy of the QPVBC membrane will facilitate low temperature fuel cell operation.

3.6. Ethanol permeability

Alcohol permeability of polymer electrolyte membranes is another determinant for potential use in ADAFCs due to its influence on the fuel cell power density, energy conversion efficiency and fuel utilization. The measurements of ethanol permeability through the QPVBC and AHA membrane, in this study, were conducted by an open circuit potential method [15–17]. In the absence of ethanol, the potential of GDE in 1 M KOH solution represents the standard electrode potential (E^{θ}). When adding the ethanol into 1 M KOH solution, the potential of GDE drops, according to the concentration of ethanol, due to the oxidation of ethanol in the Pt catalyst surface. More details about the working principle of this method has been given in a previous paper by our group [14]. The relationship between variation of GDE potential (ΔE) and ethanol concentration (c_{EtOH}) was shown in Eq. (6).

$$\Delta E = -a \ln c_{EtOH} \quad (6)$$

where a is a constant. The calibration curve of potential shift against ethanol concentration was shown in Fig. 8(a). Therefore, the ethanol concentration in compartment B during permeation experiment can be inferred from the variation of GDE potential using Eq. (6).

Relationship between the concentration of ethanol in compartment B ($c_{EtOH,B}$ in mol L^{-1}) and permeation time (t in s) was shown in Eq. (4). It is evident that $(V_B L_m / c_{EtOH,A} S) c_{EtOH,B}(t)$ has a linear correlation with the permeation time, shown in Fig. 8(b). The slope and intercept of the fitting line are ethanol permeability (P) and $P(L_m^2/6D)$, respectively. The ethanol permeability of QPVBC membrane, based on Fig. 8(b), is 3.37×10^{-11} m^2 s^{-1}, which is lower than that of AHA membrane (4.55×10^{-10} m^2 s^{-1}) when the concentration of ethanol in compartment A is 1 mol L^{-1}. The low ethanol permeability value suggested a good performance of QPVBC membrane for application in ADAFCs.

4. Conclusion

The novel pulsed after-glow discharge plasma polymerization was adopted to prepare AAEMs in this study. The TGA, ATR-FTIR and XPS analysis demonstrate that the benzyltrimethylammonium cationic groups have been successfully introduced into the polymer matrix. The content of the quaternary nitrogen in QPVBC membrane, based on XPS results, is up to 1.93 atom% due to the high preservation of functional groups in pulsed plasma polymerization progress. TGA analysis indicates that the plasma-polymerized AAEMs can be stably used below 120 °C. The satisfactory IEC (1.42 mmol g^{-1}), high percentage of benzyltrimethylammonium cationic groups, excellent hydroxide ion conductivity (0.0205 S cm^{-1} in deionized water at 20 °C) and low ethanol permeability (3.37×10^{-11} m^2 s^{-1}) suggest that such kind of plasma-polymerized AAEMs have great potential for application in alkaline directly alcohol fuel cells. Further researches on the evaluation of this type of membrane in the practical application in ADAFCs are under investigation.

Acknowledgements

This research is financially supported by the Institute of Plasma Physics, Chinese Academy of Sciences (Nos. Y05FCQ1128; 095GZ1156Y), the National Nature Science Foundation of China (No. 10975162) and the Core-University program of Japan–China.

References

[1] J.R. Varcoe, R.C.T. Slade, Fuel Cells 5 (2005) 187–200.
[2] K. Kordesch, J.C.T. Oliveira, Int. J. Hydrogen Energy 13 (1988) 411–427.
[3] J.R. Varcoe, R.C.T. Slade, G.L. Wright, Y.L. Chen, J. Phys. Chem. B 110 (2006) 21041–21049.
[4] C. Coutanceau, L. Demarconnay, C. Lamy, J.M. Leger, J. Power Sources 156 (2006) 14–19.
[5] C. Bianchini, P.K. Shen, Chem. Rev. 109 (2009) 4183–4206.
[6] J. Pan, S. Lu, Y. Li, A. Huang, L. Zhuang, J. Lu, Adv. Funct. Mater. 20 (2010) 312–319.
[7] M.R. Hibbs, C.H. Fujimoto, C.J. Cornelius, Macromolecules 42 (2009) 8316–8321.
[8] N.J. Robertson, H.A. Kostalik, T.J. Clark, P.F. Mutolo, H.D. Abruna, G.W. Coates, J. Am. Chem. Soc. 132 (2010) 3400–3404.
[9] J. Wang, Z. Zhao, F. Gong, S. Li, S. Zhang, Macromolecules 42 (2009) 8711–8717.
[10] J.R. Varcoe, R.C.T. Slade, E.L.H. Yee, S.D. Poynton, D.J. Driscoll, D.C. Apperley, Chem. Mater. 19 (2007) 2686–2693.
[11] M.R. Hibbs, M.A. Hickner, T.M. Alam, S.K. McIntyre, C.H. Fujimoto, C.J. Cornelius, Chem. Mater. 20 (2008) 2566–2573.
[12] J. Hu, Y. Meng, C. Zhang, S. Fang, Thin Solid Films 519 (2011) 2155–2162.
[13] R.K. Nagarale, G.S. Gohil, V.K. Shahi, R. Rangarajan, Macromolecules 37 (2004) 10023–10030.
[14] Z. Jiang, Z.-j. Jiang, X. Yu, Y. Meng, Plasma Process. Polym. 7 (2010) 382–389.
[15] N. Munichandraiah, K. McGrath, G.K.S. Prakash, R. Aniszfeld, G.A. Olah, J. Power Sources 117 (2003) 98–101.
[16] J. Liu, H. Wang, S. Cheng, K.-Y. Chan, J. Membr. Sci. 246 (2005) 95–101.
[17] Z. Wu, G. Sun, W. Jin, Q. Wang, H. Hou, K.-Y. Chan, Q. Xin, J. Power Sources 167 (2007) 309–314.

[18] S. Sun, G. Zhang, D. Geng, Y. Chen, M.N. Banis, R. Li, M. Cai, X. Sun, Chem. Eur. J. 16 (2010) 829–835.
[19] N. Sundaraganesan, H. Saleem, S. Mohan, M. Ramalingam, V. Sethuraman, Spectrochim. Acta A 62 (2005) 740–751.
[20] J. Reyes-Labarta, M. Herrero, P. Tiemblo, C. Mijangos, H. Reinecke, Polymer 44 (2003) 2263–2269.
[21] D.O.H. Teare, D.C. Barwick, W.C.E. Schofield, R.P. Garrod, L.J. Ward, J.P.S. Badyal, Langmuir 21 (2005) 11425–11430.
[22] S. Rajendran, T. Uma, J. Power Sources 88 (2000) 282–285.
[23] L. Sun, Y. Du, L. Fan, X. Chen, J. Yang, Polymer 47 (2006) 1796–1804.
[24] Y. Yamaguchi, T.T. Nge, A. Takemura, N. Hori, H. Ono, Biomacromolecules 6 (2005) 1941–1947.
[25] J.C. Jung, S.-B. Park, J. Polym. Sci. Pol. Chem. 34 (1996) 357–365.
[26] E. Papirer, R. Lacroix, J.-B. Donnet, G. Nanse, P. Fioux, Carbon 33 (1995) 63–72.
[27] D. Briggs, G. Beamson, Anal. Chem. 64 (1992) 1729–1736.
[28] T.I.T. Okpalugo, P. Papakonstantinou, H. Murphy, J. McLaughlin, N.M.D. Brown, Carbon 43 (2005) 153–161.
[29] F.J. Xu, E.T. Kang, K.G. Neoh, Macromolecules 38 (2005) 1573–1580.
[30] S.B. Roscoe, S. Yitzchaik, A.K. Kakkar, T.J. Marks, Z.Y. Xu, T.G. Zhang, W.P. Lin, G.K. Wong, Langmuir 12 (1996) 5338–5349.
[31] B. Zhao, K.G. Neoh, F.T. Liu, E.T. Kang, K.L. Tan, Synthetic Met. 123 (2001) 263–266.
[32] K.L. Tan, B.T.G. Tan, E.T. Kang, K.G. Neoh, J. Mater. Sci. 27 (1992) 4056–4060.
[33] A. Welle, J.D. Liao, K. Kaiser, M. Grunze, U. Mäder, N. Blank, Appl. Surf. Sci. 119 (1997) 185–198.
[34] Z. Shi, K.G. Neoh, E.T. Kang, Biomaterials 26 (2005) 501–508.
[35] C. Chen, B. Liang, D. Lu, A. Ogino, X. Wang, M. Nagatsu, Carbon 48 (2010) 939–948.
[36] T.N. Danks, R.C.T. Slade, J.R. Varcoe, J. Mater. Chem. 13 (2003) 712–721.
[37] Y. Wu, C. Wu, T. Xu, F. Yu, Y. Fu, J. Membr. Sci. 321 (2008) 299–308.
[38] K. Matsuoka, S. Chiba, Y. Iriyama, T. Abe, M. Matsuoka, K. Kikuchi, Z. Ogumi, Thin Solid Films 516 (2008) 3309–3313.
[39] M. Kumar, S. Singh, V.K. Shahi, J. Phys. Chem. B 114 (2010) 198–206.